

SHAPING THE GLOWING EYE PLANETARY NEBULA, NGC 6751

D. M. CLARK, MA. T. GARCÍA-DÍAZ, J. A. LÓPEZ, W. G. STEFFEN, AND M. G. RICHER

Instituto de Astronomía, Universidad Nacional Autónoma de México, Campus Ensenada, Ensenada, Baja California, 22800, Mexico;
dmclark@astro.unam.mx, tere@astro.unam.mx, jal@astro.unam.mx, wsteffen@astro.unam.mx, richer@astro.unam.mx

Received 2010 February 23; accepted 2010 August 24; published 2010 September 28

ABSTRACT

NGC 6751 is a highly structured multiple-shell planetary nebula (PN) with a bipolar outflow. In this work, we present a comprehensive set of spatially resolved, high spectral resolution, long-slit spectra and deep imaging from San Pedro Mártir, Gemini, the H α composite full sky survey and archive images from the *Hubble Space Telescope* and *Spitzer*. This material allows us to identify all the main morphological components and study their detailed kinematics. We find a thick equatorial structure fragmented into multiple knots that enclose a fast expanding bubble with a filamentary surface structure. The knotty ring is surrounded by faint emission from a disk-like envelope. Lobes with embedded filaments form a bipolar outflow. The equatorial ring is tilted with respect to the line of sight and with respect to the bipolar outflow. A spherical halo surrounds the PN and there is material further out identified as a fragmented outer halo. This information is used to derive a three-dimensional morpho-kinematic model using the code SHAPE that closely replicates the observed image and long-slit spectra of the nebula, providing a fair representation of its complex structure. NGC 6751 is located close to the galactic plane and its large-scale surrounding environment is shown to be a gas-rich region. We find indications that the PN is interacting with the interstellar medium. Emission components from an extended nebulosity located a couple of arcminutes away from the nebula have radial velocities that are inconsistent with the rest of NGC 6751 and are confirmed as originating from the ambient material, not related to the PN, in agreement with a previous suggestion.

Key words: ISM: jets and outflows – planetary nebulae: general – planetary nebulae: individual (NGC 6751)

Online-only material: color figures

1. INTRODUCTION

NGC 6751 is a multiple-shell planetary nebula (PN) that has attracted attention in recent years due to spectacular images obtained by the *Hubble Space Telescope* (*HST*) that reveal a highly structured inner region, earning it the “Glowing Eye” nickname. Sabbadin (1984) describes it as a possible prolate spheroid with an expansion velocity of 40 km s⁻¹. NGC 6751 was observed by Giesekeing & Solf (1986) as part of their pioneering work on bipolar, collimated outflows in planetary nebulae (PNe). They found a bipolar mass outflow oriented at a P.A. $\sim 100^\circ$ embedded in an outer envelope. The observed radial velocity of this bipolar outflow is $\sim \pm 30$ km s⁻¹ with respect to the systemic velocity and apparently slower than the expansion velocity of the main shell. Their data were insufficient to derive a spatial model though they estimate from general arguments an inclination angle of 65° with respect to the line of sight for an outflow velocity of $\sim \pm 70$ km s⁻¹. Hua & Louise (1990) in their search for haloes in PNe detected an extended filamentary nebulosity approximately 2 arcmin to the northeast of NGC 6751 and tentatively identified this material as part of a halo related to the PN, though they warned that additional evidence confirming the physical link between the extended nebulosity and the PN was needed. Chu et al. (1991) analyzed the different components of the nebula and found differences in the kinematics and the He/H ratio of the extended nebulosity with respect to the main nebula that lead them to suggest it as part of the local interstellar material. The central star of NGC 6751 has Wolf-Rayet (W-R) characteristics (Aller 1976). Chu et al. (1991) classify it as a hydrogen-deficient WC 4-type star. Koesterke & Hamann (1997) confirm this classification and derive from NLTE models a stellar temperature $T_* \simeq 140$ kK, and assume a luminosity $\log L/L_\odot = 5000$ to derive a stellar radius $R/R_\odot =$

0.13 and a mass loss rate $\dot{M} \sim 10^{-6} M_\odot \text{ yr}^{-1}$. The stellar surface composition is dominated by helium and carbon, which lead these authors to suggest the possible occurrence of a late thermal pulse. Stanghellini & Pasquali (1995) point out that the evolutionary and dynamical timescales between the shells seem significantly different and also suggest a possible born-again scenario.

In this work, we present the most comprehensive kinematic study of NGC 6751 to date. A total of nine spatially resolved, high-resolution long-slit spectra have been obtained over the main body of NGC 6751, its bipolar outflow system, the inner and detached outer haloes, and the extended nebulosity located to the northeast of the PN. The spectroscopic data are combined with imaging from *HST*, San Pedro Mártir (SPM), and a deep Gemini image that for the first time permit a complete morphological identification of the kinematic components identified spectroscopically. The spectroscopic and imaging information are used to produce a three-dimensional morpho-kinematic model of the nebula using the program SHAPE (Steffen & López 2006). Kinematics together with *Spitzer* and SASHA imagery are used to reaffirm the origin of the extended nebulosity as part of the gas-rich, local interstellar environment. This paper is organized as follows. Section 2 describes the observations, Section 3 discusses the results, Section 4 presents the SHAPE model of the nebula, and we finish with the conclusions in Section 5.

2. OBSERVATIONS

High-resolution spectroscopic observations and monochromatic images of NGC 6751 were obtained at the Observatorio Astronómico Nacional at SPM, Baja California, México on two observing runs, 2006 September 10 and 2008

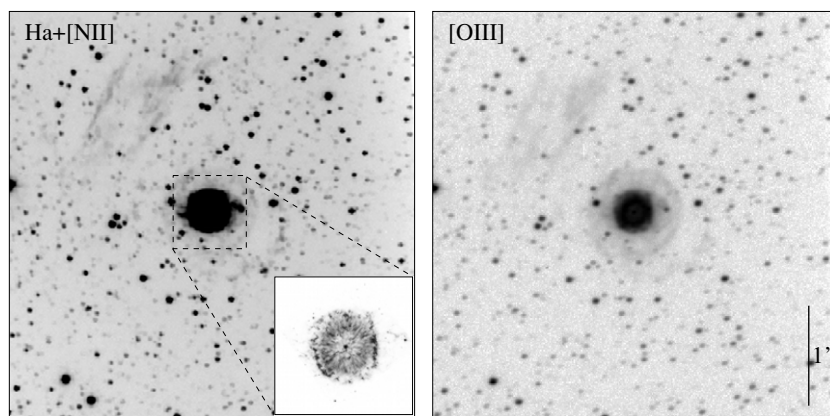


Figure 1. Deep, $H\alpha+[N II]$ and $[O III]$ images of NGC 6751 obtained at SPM. The inset shows an *HST* image of the nebula that shows its complex inner structure. North is up and east is to the left. Note the two prominent twisted filaments to the east and west of the nebula in the $H\alpha+[N II]$ image, also discernible in the *HST* image. The inner halo is apparent in the $[O III]$ image.

September 7–9. The observations were obtained with the Manchester Echelle Spectrometer (MES-SPM; Meaburn et al. 2003) on the 2.1 m telescope in its $f/7.5$ configuration. The instrument was equipped with the SITE-3 CCD detector consisting of 1024×1024 square pixels, each $24 \mu\text{m}$ on a side. We used a 90 \AA bandwidth filter to isolate the 87th order containing the $H\alpha$ and $[N II]$ $\lambda\lambda 6548, 6584$, nebular emission lines. Two-by-two binning was employed in both the spatial and spectral directions. Consequently, 512 increments, each $0''.624$ long gave a projected slit length of $5'.32$ on the sky. We used a slit $150 \mu\text{m}$ wide ($\equiv 11 \text{ km s}^{-1}$ and $1''.9$). During the observations the slit was oriented at slightly different position angles along the bipolar outflow, specifically, $97^\circ.5$, $99^\circ.5$, and 101° and one pointing at P.A. = 0° across the center of the nebula. Narrow-band images in the light of $H\alpha$ and $[N II]$ and $[O III]$ $\lambda 5007$ were also obtained with MES-SPM in its imaging mode. All spectra and images were acquired using exposure times of 1800 s. The spectra were calibrated in wavelength against the spectrum of a Th/Ar arc lamp to an accuracy of $\pm 1 \text{ km s}^{-1}$ when converted to radial velocity. The data were reduced using IRAF¹ routines, to correct bias, remove cosmic rays, and wavelength-calibrate the two-dimensional spectra. All spectra presented in this paper are corrected to heliocentric velocity (V_{hel}).

Additional material. A deep Gemini image obtained with GMOS in its imaging mode has been made available to us by Christopher Onken from the Australian Gemini Office (Gemini Program ID GS-2009A-Q-22, PI: Terry Bridges). This image is the result of the winning entry in the 2009 Gemini School Astronomy Contest, submitted by high school student Daniel Tran. Image credits are Daniel Tran (PAL College), Travis Rector (University Alaska Anchorage), Terry Bridges (Queen’s University), and the Australian Gemini Office. The original color image (<http://www.gemini.edu/node/11329>) received 1 hr of Gemini telescope time and is the result of combining narrowband images obtained in the light of $H\alpha$, $[S II]$, and $[O III]$. The *HST* image of NGC 6751 was obtained from the STScI Web site and is part of the Hubble Heritage Team collection.² Images from the $8 \mu\text{m}$ IRAC *Spitzer*³ work survey were obtained from

their archive. A wide field 25° , $H\alpha$ image from the $H\alpha$ full sky map (Finkbeiner 2003), was obtained from the SkyView web tool.

3. RESULTS AND DISCUSSION

3.1. Morphology

Figure 1 shows two deep images of NGC 6751 obtained with MES-SPM in its imaging mode in the light of $H\alpha+[N II]$ and $[O III]$. The $H\alpha+[N II]$ image shown here is saturated in the central region in order to highlight the seemingly point-symmetric filaments on the west and east side of the main shell. The $[O III]$ image clearly exhibits a bright rim and a surrounding spherical halo with a radius of $27''$ that incidentally corresponds to the “outer envelope” described by Giesekeing & Solf (1986). Outside of the $27''$ inner halo, there is additional emission corresponding to an outer halo in the form of a broken filament at a radius of $\sim 44''\text{--}50''$. In addition, extended filamentary nebulosity can be appreciated up to nearly $2'$ away to the north and northeast of the PN in both images. The inset in the $H\alpha+[N II]$ image contains the *HST* image with the same orientation showing the opposite outflows and the bright, knotty structure that encircles the rich filamentary central bubble.

Figure 2 shows the gray-scale version of the superb Gemini image where all the elements described in Figure 1 can be clearly seen. Of particular relevance are the faint bipolar lobes that surround the filaments and are clearly revealed here for the first time. The filaments that appear as point symmetric in Figure 1 are embedded in the lobes, the latter correspond to the “puzzling oval” described by Chu et al. (1991).

3.2. Kinematics

In Figure 3 we present the deep, $H\alpha+[N II]$ image of NGC 6751 taken at SPM overlaid with the nine slit positions we observed. The right panel of this figure shows the location of the slits on the *HST* image for a better visualization of their location over the central region of the nebula.

Figure 4 presents the position–velocity (P – V) arrays corresponding to the $[N II]$ line profiles for each slit position. In each case, the corresponding synthetic P – V array derived from the SHAPE model (see the next section) is shown next to the observed line profile (see Figure 9, panel (f), for component labels). In slit (a) (top left in Figure 4), the emission located at offset $165''$ is from the local interstellar medium (ISM; see Figure 7,

¹ IRAF is distributed by the National Optical Astronomy Observatory, which is operated by the Association of Universities for Research in Astronomy, Inc., under cooperative agreement with the National Science foundation.

² *HST* image credit: NASA, ESA, and the Hubble Heritage Team (STScI/Aura).

³ The *Spitzer Space Telescope* is operated by the Jet Propulsion Laboratory, California Institute of Technology under contract with NASA.



Figure 2. Gray-scale version of the Gemini image of NGC 6751 the original color-coded image is the result of separate exposures in the light of H α , [S II], and [O III] and is shown in the electronic version. This image shows clearly for the first time all the structural components of this complex nebula, as described in the text (and see also Figures 5 and 7 where these components are labeled). Image credits are Daniel Tran (PAL College), Travis Rector (University of Alaska, Anchorage), Terry Bridges (Queen’s University), and the Australian Gemini Office (<http://www.gemini.edu/node/11329>).

(A color version of this figure is available in the online journal.)

panel (b)) as discussed below, and the one at offset 115'' is from the outer halo, the model does not include these structural components. Figure 4 includes all observed positions except position b, which is shown in Figure 7. Slit (a) is at a P.A. of 0° with north at the top and south at the bottom of the *P*–*V* profile in the figure. Slits (b) and (c) are at a P.A. of 101°, slits (d)–(g) at a P.A. of 97°.5, and slits (h)–(i) at a P.A. of 99°.5. In these slits the western side is at the top of the line profile and the eastern side at the bottom of the *P*–*V* profiles in the figure. The

unprecedented coverage of the long-slit spectra together with the Gemini and *HST* images allow us to separate the constituent parts of the nebula and study them individually.

In Figure 5, we present a mosaic with each panel highlighting different components of NGC 6751. In each panel are indicated the slit positions corresponding to the relevant component, i.e., the outer halo, the inner halo, the filamentary, bipolar lobes, and the knotty ring. The information corresponding to the extended nebulosity is shown separately in Figure 7 since, as discussed below, this material shows evidence of not being part of the PN. The length and positions indicated for the slits in Figure 5 show the approximate location of the slit and the spatial extent along which kinematic data have been extracted. The kinematic data for each panel in Figure 5 are presented in Table 1. The corresponding data for the slits indicated on the right panel in Figure 7 are indicated directly on that figure. The velocities of the central bubble, corresponding to the velocity ellipsoids apparent in the line profiles in Figure 4 (and Figure 6, see below), are listed directly in Table 1.

The heliocentric systemic velocity of NGC 6751 is measured at $V_{\text{sys}} = -31.7(\pm 2) \text{ km s}^{-1}$, derived from both slits (g) and (a) that pass through the central star (see Figure 6). This value is lower than those quoted by Chu et al. (1991) and Sabbadin (1984) of $V_{\text{sys}} = -42$ and -39 km s^{-1} , respectively. The origin of this difference is unclear.

One can easily discern the distinct kinematic signature of each component of NGC 6751 from Table 1. The outer halo is characterized by heliocentric velocities of the order of $V_{\text{hel}} \simeq -15 \text{ km s}^{-1}$ whereas the inner halo shows values of $V_{\text{hel}} \simeq -31 \text{ km s}^{-1}$ on average. The bipolar lobes show distinct expansion velocities with the blueshifted side at about $V_{\text{hel}} = 0 \text{ km s}^{-1}$ and the redshifted one at $V_{\text{hel}} = -62 \text{ km s}^{-1}$, average values. For slits (d)–(f), we were able to measure the velocity of the lobes for regions close to but outside the brighter filaments, these values are listed as the second row of values in Table 1 for those slits. The lobe velocities are very similar to those of the filaments. This coincidence in velocities indicates that the filaments and lobes are part of the same bipolar outflow, i.e., the filaments do not seem to represent high-velocity elements advancing through a slower moving envelope formed by the lobes, as is sometimes observed in some PNe, but rather seem to be denser filaments than the surrounding material, embedded in the bipolar outflow and flowing as part of the lobes. The Gemini image provides some hints that indicate that these denser filaments run predominantly along opposite walls of the bipolar

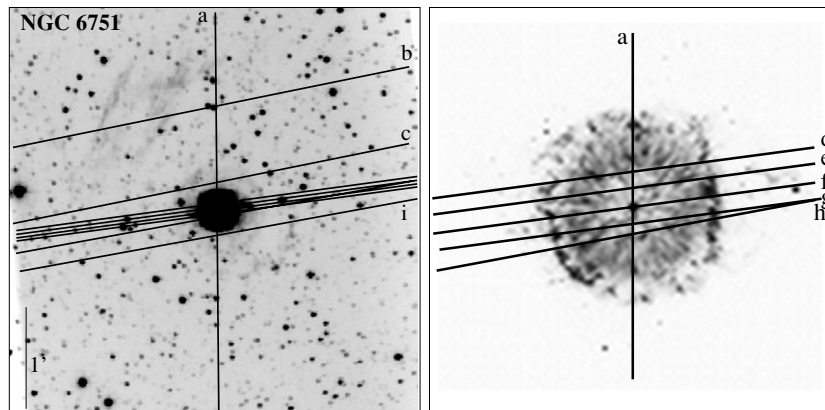


Figure 3. Left panel: the positions of the long slits are indicated against a deep, H α + [N II] image of NGC 6751 obtained at SPM. North is up, east is to the left, and the image scale is shown at the lower left. Right panel: the *HST* image is used to show more clearly the location of the central long slits over the lobes, knotty ring, and filamentary central bubble in this confined area. The *HST* image covers $\approx 1' \times 1'$.

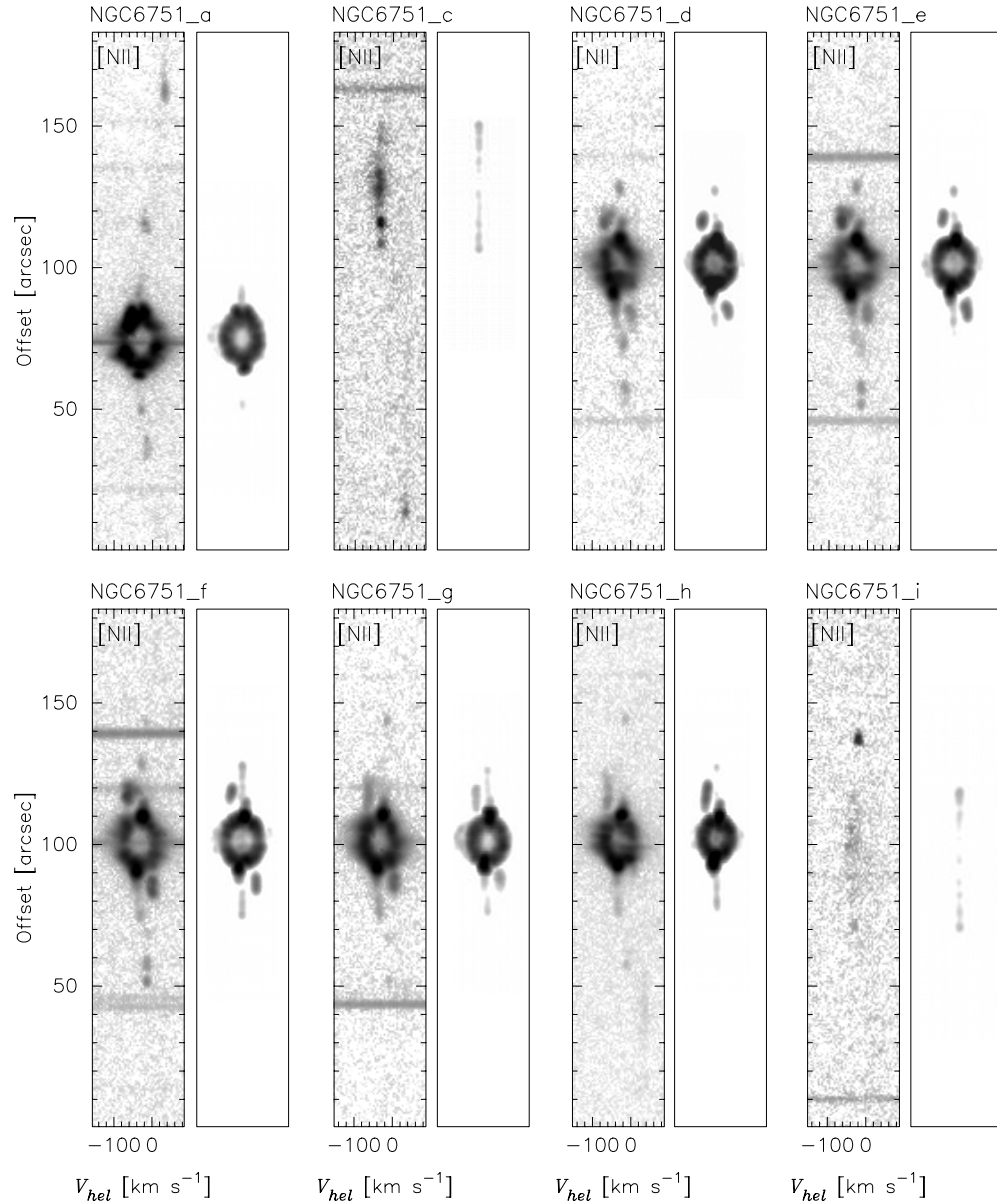


Figure 4. For each slit position there is a pair of P - V arrays, the observed $[\text{N II}]\lambda 6583$ line profile on the left and the corresponding synthetic P - V array modeled with SHAPE on the right side. The P - V array corresponding to slit position (b) is shown in Figure 7. See Figure 9, panel (f), for component labels. The SHAPE model does not include the outer halo. For slit (a), north is at the top and south at the bottom, for all the others, west is at the top and east at the bottom of the P - V array.

Table 1
 V_{hel} for the Different Components of NGC 6751

Slit	Outer Halo V_{hel} (km s^{-1})	Inner Halo V_{hel} (km s^{-1})	Bipolar Lobes V_{hel} (km s^{-1})	Ring Knots V_{hel} (km s^{-1})	Bubble V_{hel} (km s^{-1})
(a)	-19.3; -15.3	-35.8; -30.3	...	-23.5, -53.5; -34.8	+11.2; -73.6
(c)	...	-31.5, -33.3, -35.6, -31.9
(d)	-14.3; ...	-19.8; -28.4	-3.4; -65.8 +1.6; -59.4	-44.4; -27.5	+0.7; -63.5
(e)	-15.6, -16.1; ...	-33.9; -27.9	-1.0; -65.3 ... ; -58.9	-43.0; -27.0	+6.7; -72.1
(f)	-12.8, -13.7; -16.4	-31.0; -27.4	-0.5; -63.4 ... ; -61.1	-40.6; -24.6	+9.1; -73.4
(g)	-8.9, -10.2; -14.8	-33.9; ...	+3.4; -61.3	-39.4; -24.4	+5.2; -70.9
(h)	-11.3 ... ; -15.0	-33.2; ; -60.1	-34.1; -24.1	+2.4; -67.4
(i) ; -18.7	-28.2, -35.1, -31.0, -44.6, -35.1, -30.5

Notes. V_{hel} measured for the segments of the slits indicated in Figure 5. The measurements are listed north first then south for slit (a) and from east to west for all other slits. Values measured on one side of the nebula are separated from the other side by a semicolon.

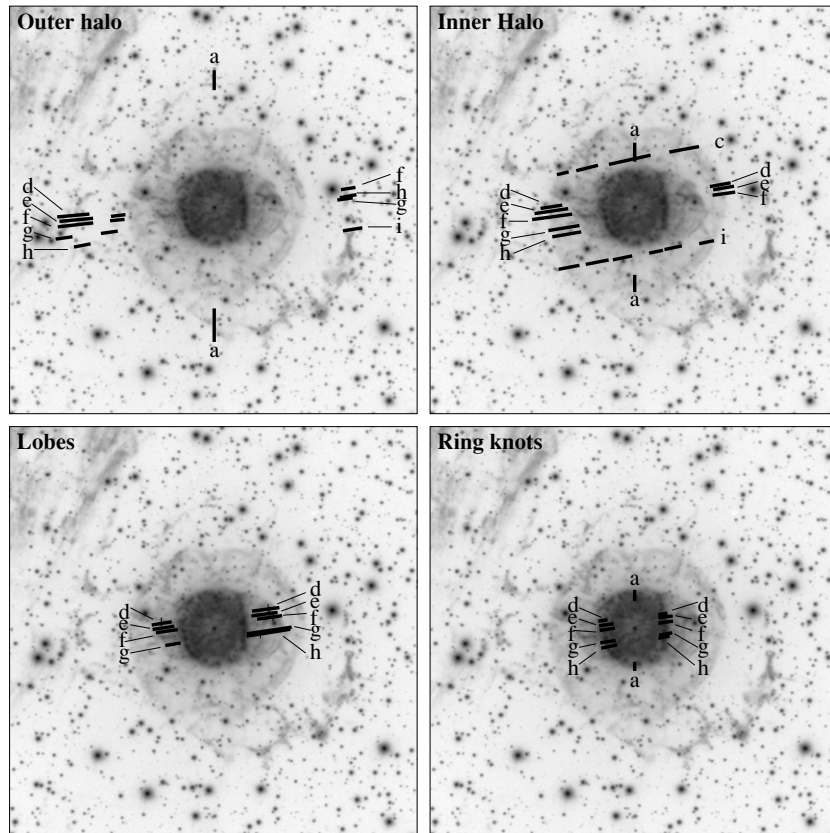


Figure 5. Slit positions and length over which kinematic data are extracted and tabulated in Table 1 are indicated in each panel for different main components of NGC 6751, as indicated in each panel.

lobes, producing the point-symmetric shape apparent in ground-based images (e.g., see the $H\alpha+[N II]$ image in Figure 1) such as in the case of the bipolar PN Hb 5.

A system of knotty structures defines a ring that encircles the central bubble (see Figure 6), the velocities of these knots have predominantly radial motion away from the central star, following the velocity ellipsoid of the central bubble and are located at its outer border. Opposite knots in the ring show however a clear velocity difference between the east and west sides, the eastern side shows an average velocity $V_{\text{hel}} \simeq -40 \text{ km s}^{-1}$ and the western side a $V_{\text{hel}} \simeq -26 \text{ km s}^{-1}$, indicating a tilt in the ring with respect to the line of sight, with the eastern side on the near side and the western part on the far side. An additional indication of the spatial orientation of the ring is given by the systematic decrease in values from top (north) to bottom (south) in the ring, apparent in Table 1, suggesting that the top (north) of the ring is also tilted forward.

The expansion velocities of the central bubble show the expected monotonic decrease in values from the slits located away from the center, though there is some deviant behavior from the smooth velocity ellipsoid that would represent a spherically expanding bubble in some cases, such as slit (d). The average expansion velocity of the central bubble, taken as half the peak-to-peak velocity difference from the values listed in Table 1 for slits (a) and (f) that cross the center of the nebula, yields $\simeq 42 \text{ km s}^{-1}$, this is considered an above average expansion value for a PN (e.g., Richer et al. 2010).

For a further scrutiny of the kinematics of NGC 6751, a close-up of the six $P-V$ line profiles from the central region of the nebula (slits (a), (d), (e), (f), (g), and (h), see Figure 3) is presented in Figure 6. In these panels, one can identify

the main components of the inner regions of the PN that we have already discussed, namely, the velocity ellipsoid from the central expanding bubble, the conspicuous, bright knots from the surrounding ring located at the external border of the velocity ellipsoid, and the bipolar lobes located outside the velocity ellipsoid showing opposite velocities (see Figure 9, panel (f), for an identification of these components on the synthetic $P-V$ array of slit (g)). Moreover, additional condensations are apparent in the $P-V$ line profiles in Figure 6, along the walls of the velocity ellipsoid, indicating that these are series of dense regions at the surface of the highly structured expanding shell (see the right panel in Figure 3). The $P-V$ arrays in this figure also reveal that the emission from the knots is always accompanied by faint radial extensions that appear to be emission from a disk-like envelope to this ring, perhaps formed by photoevaporated material and stellar wind overrunning the ring of knots. Also, we detect an additional high-velocity component that manifests itself as faint, diffuse emission located between the spatial offsets that enclose the central expanding shell. It doubles the expansion velocity described by the velocity ellipsoid, i.e., it runs approximately from $V_{\text{hel}} \simeq -120$ to $+60 \text{ km s}^{-1}$.

As for the extended nebulosity, values shown in Figure 7, panel (b), indicate velocities of the order of $V_{\text{hel}} \simeq +29 \text{ km s}^{-1}$, this velocity is very different from the rest of the nebula and a strong indication that this gas is unrelated to the PN. Further evidence in this regard is substantiated by examining the surroundings of NGC 6751. Panel (a) in Figure 7 shows a mosaic from the *Spitzer* Infrared Array Camera $8 \mu\text{m}$ images that reveals that the extended diffuse emission seen to the northeast of NGC 6751 continues extending at least $10'$ to the north. Panel (c) shows a much wider $30^\circ \times 30^\circ$ field of view of

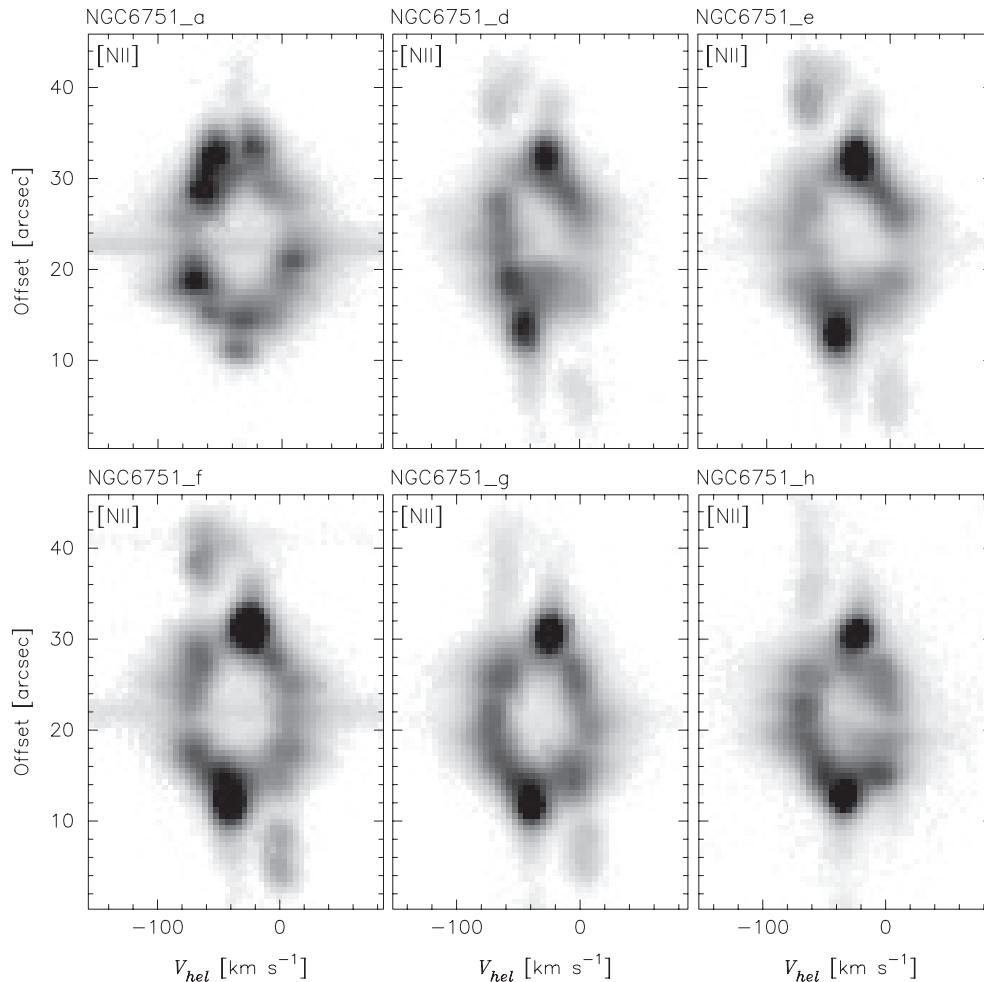


Figure 6. Close-up view of the six [N II] P - V line profiles from the central region of the nebula. The data are displayed with a square root intensity scale to show at the same time the bright ring knots and the faint, high-velocity material and other components discussed in the text. The continuum from the central star is apparent in the panels for slits (a) and (f) (top and bottom left).

the region from the $H\alpha$ composite full sky map (Finkbeiner 2003) with separate zoom levels at $15^\circ \times 15^\circ$ and $5^\circ \times 5^\circ$ around the position of NGC 6751 that make it clear that this PN is embedded in a gas-rich environment within the disk of the Milky Way. The present results together with those from Chu et al. (1991) provide plausible evidence that this extended nebulosity is unrelated to NGC 6751.

Table 2 lists the average expansion velocities measured from the different components of NGC 6751 with respect to the systemic velocity $V_{\text{sys}} = -31.7 \text{ km s}^{-1}$, i.e., $V_{\text{exp}} = V_{\text{hel}} - V_{\text{sys}}$, their corresponding radii, and kinematic timescales. A distance of 2 kpc (Chu et al. 1991) has been adopted. These velocities provide the expansion pattern of the material with respect to the nebula's reference frame, without considering projection effects. The values in Table 2 indicate that the outer halo is receding from the nebula, whereas the inner halo is essentially inert. The bipolar lobes have a projected outflow velocity of $\pm 31 \text{ km s}^{-1}$ (in good agreement with the values derived by Gieseking & Solf 1986). Table 2 also lists in parenthesis the deprojected velocity for the bipolar outflow considering a tilt of 23° with respect to the plane of the sky derived from our model (see below). The central bubble expands at 41.8 km s^{-1} and the knotty ring that surrounds it shows a velocity asymmetry (-8.3 km s^{-1} on the east side and $+5.7 \text{ km s}^{-1}$ on the west side) that is interpreted as a projection effect due to a tilt of the ring with respect to the sightline. The model derived tilt for the

Table 2
Average Expansion with Respect to V_{sys} , Dimensions, and Timescales

Component	$V_{\text{exp}} = V_{\text{hel}} - V_{\text{sys}} (\text{km s}^{-1})$	Radius ($''$)	t (yr)
Outer halo	+16.9	50	
Inner halo	2	27	1.28×10^5
Bipolar lobes	$\pm 31 (\pm 79)$	21	2.80×10^3
Central bubble	41.8	12	2.72×10^3
Ring knots	7(40)	22	5.13×10^3
Diffuse high velocity	± 90	16	1.69×10^3
Extended nebulosity	+58.7	114	

Notes. Deprojected velocities are listed within parenthesis. For the bipolar lobes, a tilt with respect to the plane of the sky of 23° is considered and 10° for the ring. A distance of 2 kpc to NGC 6751 has been adopted.

ring is 10° , and the deprojected value in this case is also shown in parenthesis. The high-velocity, faint, diffuse material that engulfs the ring and central bubble expands at $\approx \pm 90 \text{ km s}^{-1}$, and finally the extended nebulosity located to the northeast of the nebula shows a large receding velocity of $+59 \text{ km s}^{-1}$ in clear disagreement with the values of the other components related to the nebula.

4. SHAPE MODELING

To understand the complex three-dimensional structure and kinematics of NGC 6751, we used the program SHAPE (Steffen

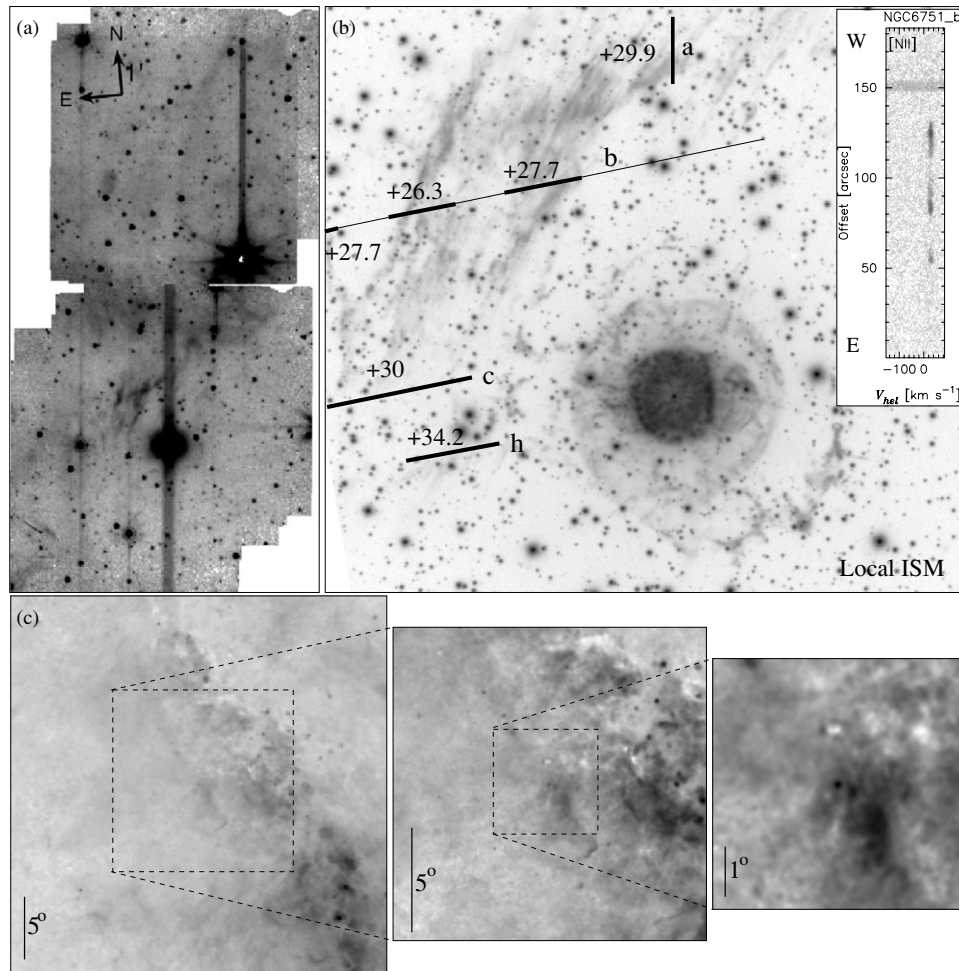


Figure 7. Panel (a): a mosaic of two *Spitzer* IRAC 8 μm fields showing a wide field around NGC 6751, which is the bright source in the bottom half of the panel. The image is saturated and the gray-scale level emphasized to bring out the faint, filamentary emission seen near this PN. The compass at the upper left corner shows the orientation, and the length of each arrow is $1'$. Panel (b): the slit positions and length over which kinematic data are extracted in the extended nebulosity. The corresponding values of V_{hel} are indicated in the figure. The P - V array for slit (b) is shown in the top right corner. Panel (c): a wide field $\text{H}\alpha$ image taken from the $\text{H}\alpha$ composite full sky map (Finkbeiner 2003) for three, separate zoom levels around the position of NGC 6751. The PN can be seen as the small, black dot at the center of the last zoom level.

& López 2006). SHAPE is a morpho-kinematic modeling tool that allows the user to reconstruct the three-dimensional structure and observed spectral line profiles using diverse geometrical forms. SHAPE uses as reference monochromatic images and observed P - V diagrams to reproduce the three-dimensional structure and kinematics of the object. Particles are distributed over a surface, or throughout a specified volume, and are assigned a specific velocity law and relative brightness. Several particle systems can be used and each can be assigned different velocity laws to form a complex object. The resultant two-dimensional image and spectral information are then rendered from the three-dimensional model and compared with the real data. A key advantage of SHAPE for objects like NGC 6751 is its ability to model independent structures, each with its own velocity law, and then merge them into a single product. We have used velocity laws of the Hubble-type $v = k \cdot r/r_o$, where k is a constant, r is the distance from the source, and r_o is the distance at which the velocity k is reached. The values for k and r_o have been chosen to match the observed velocities for the various components of NGC 6751 and to provide reasonable distance scales along the line of sight.

The SHAPE analysis presented here is similar to the one performed by García-Díaz et al. (2009) for NGC 6337. We

use the observed $[\text{N II}]P$ - V line profiles since they contain all of the main components. The model consists of five main parts: the inner halo, the bipolar outflow, a fragmented ring, a disk exterior to the ring, and a central bubble with a high-velocity component. The model does not include the outer halo. The wire-frame model, before rendering, is shown in Figure 8 where six views at different orientations (from 0° to 90° in 15° intervals) are shown. We assume that these structures obey a Hubble-type velocity law, except for the bubble and inner halo where we used a constant velocity. Particles were distributed on the surface of a sphere for the inner halo and within a volume for the bubble. For the high-velocity component, we assigned a higher velocity to the corresponding set of particles. The ring and disk are inclined by $10^\circ \pm 5^\circ$ with respect to the plane of the sky (western side into the plane of the sky) and exhibit a slight warp about the north-south axis. The bipolar lobes' system are formed by curved surfaces that describe the walls of the opposite lobes along which run the bright filaments that produce a point-symmetric appearance in the outflow. From the model, we derived a position angle for the bipolar outflow of $97:5$ ($277:5$) $\pm 10^\circ$ with an inclination of $23^\circ \pm 5^\circ$ with respect to the plane of the sky.

The results of the final rendered SHAPE model are shown in Figure 9, where they are compared with the basic morphology of

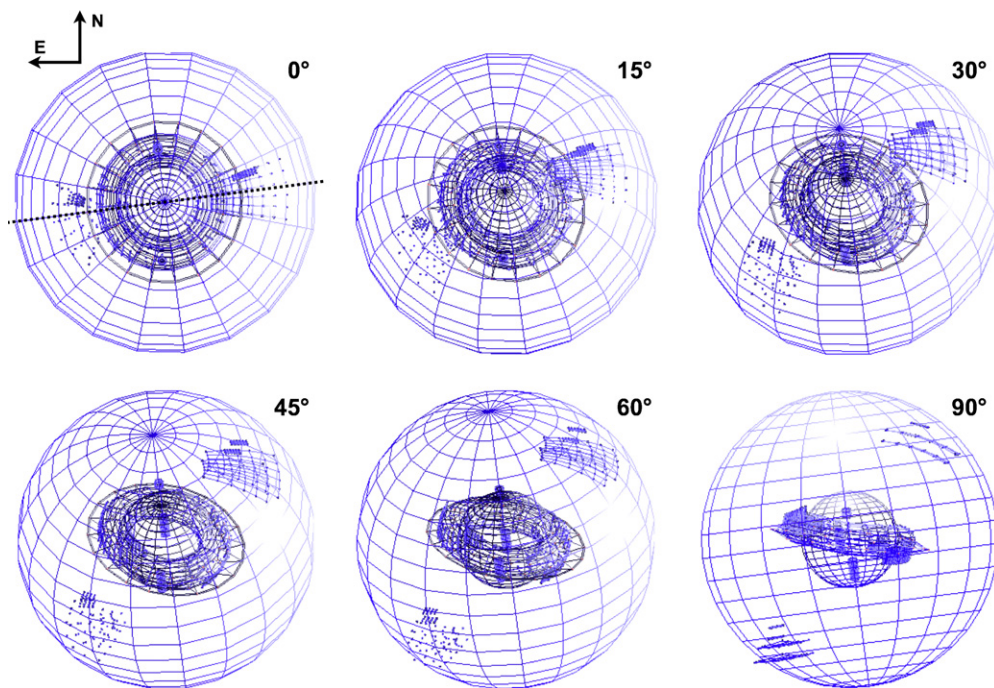


Figure 8. Six views of the SHAPE mesh model before rendering. On the top left is the view as seen by the observer with north up and east to the left. In each successive frame, the model has been rotated into the page by the degrees specified to the upper right. The axis of rotation is about the dotted line shown in the first image. The outer sphere represents the inner halo and has a uniform distribution of particles (uniform emissivity). The ring and its surrounding disk are best seen in the view tilted by 45° or 60°. The central bubble is most clearly seen in the view tilted by 90°. The high-velocity component is not shown but is within the bubble. The bipolar outflow, depicted by its opposite outermost segments, is best seen in the same view tilted at 90°. In this same view, the particles within the bubble, above and below the ring, represent the condensations seen in the inner regions of the velocity ellipsoids in Figure 6. (A color version of this figure is available in the online journal.)

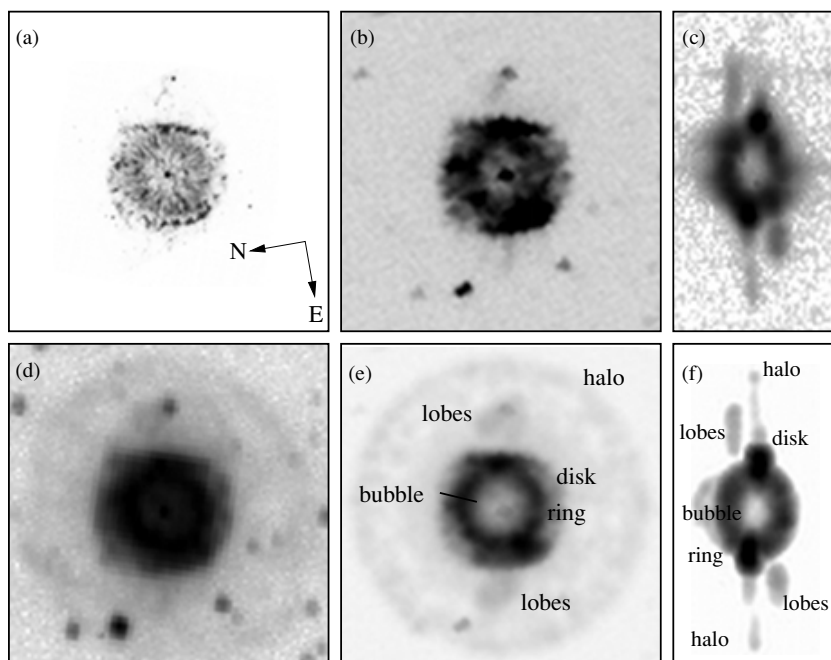


Figure 9. Comparisons between observations of NGC 6751 and the SHAPE models of this nebula. (a) *HST* image, (b) $H\alpha + [N II]$ image from SPM, (c) the observed, $[N II]$ profile for slit (g), (d) SPM, $[O III]$ image, (e) the SHAPE model image, and (f) the synthetic, SHAPE spectrum for slit (g). In (e) and (f), we label the various components of the nebula that we discuss in this paper. The high-velocity component is also present but it is not labeled here. All images are 1'1 × 1'1. The orientation of the images is shown in panel (a).

NGC 6751 and the observed $P-V$ line profiles (see also Figure 4). The noise-like texture in the synthetic image is the result of the rendering process over the finite distribution of surface particles in the image. Panel (a) is the *HST* image and panel (b) is the $H\alpha + [N II]$ MES-SPM image. Panel (c) shows the observed

$P-V$ array from slit position (g) that runs throughout the lobes. Panel (d) is the $[O III]$, MES-SPM image. The rendered, model image is in panel (e) and the rendered model spectrum for slit position (g) is in panel (f). Five main features of NGC 6751 are indicated in the last two panels. The images in this figure are

rotated $\sim 97^\circ$ counterclockwise with approximately west up and north to the left to approximately match and ease comparison of morphological elements of the nebula with emission features in the P - V arrays here and in Figures 4 and 6. The exact orientation of these images is indicated in panel (a).

The present SHAPE model successfully represents the main characteristics of the complex “Glowing Eye” nebula. It is able to reproduce the basic two-dimensional morphology and the set of complex emission line profiles that provide a representation of the third dimension of the nebula through the radial velocity component. A limitation of the model is that it cannot place restrictions on, for example, the exact shape of the inner halo and the central bubble, which have been assumed spherical though a slightly prolate form is likely. In addition, the velocity ellipsoid from the central bubble is distorted in some sections due to the presence of condensations, such as filaments and knots in the inner regions of the bubble or at its surface. The model cannot disentangle the detailed differences that these distortions produce in shape but this effect is in any case of minor consequence for the overall result. The model can neither constrain the length of the bipolar outflow, which is considered to remain within the boundaries of the inner halo, nor the thickness of the toroid. As discussed above, the inner halo and central bubble are considered spheres expanding at constant velocity, while the other components are geometrical forms whose particles follow a Hubble-type velocity law ($v = k \cdot r/r_o$), therefore, given various values of k , one can vary the distance, r , for a particular part of the nebula and achieve a similar observed velocity. Thus, slightly different geometric forms could have been used to build up the final model, but in the end there is only a very limited set of solutions that are able to replicate the complex P - V diagrams of NGC 6751.

5. DISCUSSION

We have derived a morpho-kinematic model for NGC 6751 that is able to replicate the main morphological and kinematic components of this nebula and provides a good understanding of its complex structure and outflows that otherwise are rather difficult to visualize given its projected orientation on the sky. We find six distinct structural and kinematic components in NGC 6751: outer and inner haloes, filamentary bipolar lobes, a central bubble surrounded by a knotty ring, and diffuse high-velocity gas.

The values in Table 2 indicate that the outer halo is receding from the nebula whereas the inner halo is essentially inert. The filaments that form the outer halo are most probably related to the earliest stages of mass loss during the asymptotic giant branch (AGB) stage, and their current overall receding velocity is probably due to its extended interaction with the local ISM which tends to drag away this material, these conditions prevent an estimate of its kinematic timescale.

The inner halo must have been produced in a later mass-loss episode. It has a notably low expansion velocity indicating that the fast stellar wind is still mostly contained within the pressure-driven central bubble.

A bipolar outflow emerges at an angle with respect to the plane of the ring, with dense filaments embedded in the lobes. The filaments delineate a point-symmetric pattern apparent in ground-based images. The filaments and lobes have similar outflow velocities. The bipolar lobes have a projected outflowing velocity of $\pm 31 \text{ km s}^{-1}$ in good agreement with the values derived by Giesekeing & Solf (1986). A tilt of 23° with respect to the plane of the sky is derived from our model which

yields a deprojected velocity ($\pm 79 \text{ km s}^{-1}$) for the bipolar outflow.

The central bubble expands at 41.8 km s^{-1} , and the knotty ring that surrounds it shows a velocity asymmetry that is interpreted as a projection effect due to a tilt of the ring with respect to the plane of the sky. The model-derived tilt for the ring is $\sim 10^\circ$ and the deprojected expansion velocity of the ring results in $\sim 40 \text{ km s}^{-1}$, which closely matches that of the central bubble, indicating that the expansion of the ring is likely being driven by the pressure from the bubble. Faint emission extending outward from the knots is detected in the spectra and this is identified with a disk-like extension to the knotty ring, following the same kinematic pattern. This disk-like structure is possibly related to ablated material from the knots by the erosive action of the percolating stellar wind and photoevaporation processes producing a radial mass-loaded outflow from the knots.

The high-velocity, faint, diffuse material that engulfs the ring and central bubble expands at $\approx \pm 90 \text{ km s}^{-1}$ and is most likely material directly related to the fast wind that is starting to percolate through the central regions.

The timescales that result from our model indicate that the inner halo formed some 10^5 years ago while the bipolar lobes, the central bubble, and the knotty ring occurred approximately simultaneously, some $(3-5) \times 10^3$ years ago, whereas the diffuse, faint, high-velocity component must be more recent. The outer filamentary halo is presumably related to the mass lost during the AGB stage and as such is the oldest structure of this PN, currently showing kinematic signs of an extended interaction with the local ISM. The contrasting kinematic differences between the halos and the other structures lend credence to the hypothesis that NGC 6751 underwent a late thermal pulse (Koesterke & Hamann 1997; Stanghellini & Pasquali 1995).

The extended nebulosity located to the north and northeast of the nebula shows a large receding velocity of $+59 \text{ km s}^{-1}$ in clear disagreement with the values of the other components related to the nebula. Considering the large-scale, gas-rich environment in which NGC 6751 is located, we conclude that the surrounding extended nebulosity is not part of the PN.

M.T.G.-D. gratefully acknowledges the support of a postdoctoral grant from UNAM. This research has benefited from the financial support of DGAPA-UNAM through grants IN116908, IN108506, and IN108406, and CONACYT grants 49447 and 82066. We acknowledge the excellent support of the technical personnel at the OAN-SPM, particularly Gustavo Melgoza and Felipe Montalvo, who were the telescope operators during our observing runs.

REFERENCES

- Aller, L. H. 1976, *Mem. Soc. R. Sci. Liege*, **9**, 271
 Chu, Y.-H., Manchado, A., Jacoby, G. H., & Kwitter, K. B. 1991, *ApJ*, **376**, 150
 Finkbeiner, D. P. 2003, *ApJS*, **146**, 407
 García-Díaz, Ma. T., Clark, D. M., López, J. A., Steffen, W., & Richer, M. G. 2009, *ApJ*, **699**, 1633
 Giesekeing, F., & Solf, J. 1986, *A&A*, **163**, 174
 Hua, C. T., & Louise, R. 1990, *A&A*, **235**, 403
 Koesterke, L., & Hamann, W.-R. 1997, *A&A*, **320**, 91
 Meaburn, J., López, J. A., Gutiérrez, L., Quiróz, F., Murillo, J. M., Valdéz, J., & Pedrayez, M. 2003, *RevMexAA*, **39**, 185
 Richer, M. G., López, J. A., García-Díaz, Ma. T., Clark, D. M., Pereyra, M., & Díaz-Mendez, E. 2010, *ApJ*, **716**, 857
 Sabbadin, F. 1984, *MNRAS*, **210**, 341
 Stanghellini, L., & Pasquali, A. 1995, *ApJ*, **452**, 286
 Steffen, W., & López, J. A. 2006, *RevMexAA*, **42**, 99